ISSN 0965-5425, Computational Mathematics and Mathematical Physics, 2016, Vol. 56, No. 6, pp. 1086–1095. © Pleiades Publishing, Ltd., 2016.
Original Russian Text © V.A. Biryukov, V.A. Miryakha, I.B. Petrov, N.I. Khokhlov, 2016, published in Zhurnal Vychislitel'noi Matematiki i Matematicheskoi Fiziki, 2016, Vol. 56, No. 6, pp. 1104–1114.

Dedicated to the memory of O.M. Belotserkovskii

Simulation of Elastic Wave Propagation in Geological Media: Intercomparison of Three Numerical Methods

V. A. Biryukov, V. A. Miryakha, I. B. Petrov, and N. I. Khokhlov

Moscow Institute of Physics and Technology (State University),
Institutskii per. 9, Dolgoprudnyi, Moscow oblast, 141700 Russia

e-mail: biryukov.vova@gmail.com, vlad.miryaha@gmail.com, petrov@mipt.ru, k_h@inbox.ru

Received November 9, 2015

Abstract—For wave propagation in heterogeneous media, we compare numerical results produced by grid-characteristic methods on structured rectangular and unstructured triangular meshes and by a discontinuous Galerkin method on unstructured triangular meshes as applied to the linear system of elasticity equations in the context of direct seismic exploration with an anticlinal trap model. It is shown that the resulting synthetic seismograms are in reasonable quantitative agreement. The grid-characteristic method on structured meshes requires more nodes for approximating curved boundaries, but it has a higher computation speed, which makes it preferable for the given class of problems.

Keywords: grid-characteristic method, discontinuous Galerkin method, seismic exploration problems.

DOI: 10.1134/S0965542516060087

INTRODUCTION

The numerical simulation of wave propagation in rock with the subsequent analysis of synthetic seismograms is a task of utmost importance in planning exploration work and field data interpretation, as well as is an integral part of the solution of inversion and migration problems. At present, numerous approaches are available; their classification can be found, for example, [1–4]. An important criterion is that the numerical method for solving the complete system of differential equations (usually the linear elasticity equations [5]) is high-order accurate. This ensures low numerical viscosity, which is necessary for wave propagation through distances of hundreds and thousands of wave lengths without wave front distortions. Accordingly, finite-difference methods (FDM), spectral element methods (SEM), and discontinuous Galerkin methods (DGM) [6–9] are usually used in computational geophysics. Examples of computations by applying the grid-characteristic method on structured and unstructured meshes can be found in [10–14].

In this paper, the following three numerical methods are compared as applied to the two-dimensional geological anticlinal trap model described in [1]:

- a discontinuous Galerkin method (DGM) on unstructured meshes [8, 15];
- a grid-characteristic method on unstructured triangular meshes (GCM Unstructured) [16, 17];
- a shock-capturing grid-characteristic method on structured meshes (GCM Structured) [18, 19].

The goal of comparison is to cross-verify the numerical methods and demonstrate the possibility of solving two-dimensional direct simulation problems in seismic exploration for near industrial formulations (in the frequency range of 10–80 Hz). We compare seismograms, individual wave paths, and the required runtime and storage.

The anticlinal trap model from [1] is used as a geological model. The Marmousi [20], Marmousi2 [21], and the SEG/EAGE salt model are also frequently chosen for comparison.

Such comparisons are rare in the literature and usually concern no more than two numerical methods. The DGM and its modifications are usually verified and compared in terms of accuracy with SEM [7, 22–24]. The comparison of SEM and DGM in [6] shows that they have a comparable runtime per one degree of

freedom, while their total number is somewhat larger in DGM. In [25] three numerical methods (FDM, SEM, Kirchhoff's) are compared in the context sea seismic exploration with a daytime surface of complex geometry. Four methods (FDM, FEM, SEM, and DGM) as applied to the simulation of seismic wave propagation in earthquakes for various P-wave to S-wave speed ratios (c_p/c_s) are compared in [26].

1. GOVERNING EQUATIONS AND NUMERICAL METHODS

The behavior of a rock medium was described using the model of an ideal isotropic linear elastic material [5]. The following system of partial differential equations describes the state of an elastic material in a volume element in the approximation of small deformations for the two-dimensional case:

$$\rho\frac{\partial v_x}{\partial t} = \frac{\partial \sigma_{xx}}{\partial x} + \frac{\partial \sigma_{xy}}{\partial y}, \quad \rho\frac{\partial v_y}{\partial t} = \frac{\partial \sigma_{xy}}{\partial x} + \frac{\partial \sigma_{yy}}{\partial y},$$

$$\frac{\partial \sigma_{xx}}{\partial t} = (\lambda + 2\mu)\frac{\partial v_x}{\partial x} + \lambda\frac{\partial v_y}{\partial y}, \quad \frac{\partial \sigma_{yy}}{\partial t} = \lambda\frac{\partial v_x}{\partial x} + (\lambda + 2\mu)\frac{\partial v_y}{\partial y}, \quad \frac{\partial \sigma_{xy}}{\partial t} = \mu\left(\frac{\partial v_x}{\partial x} + \frac{\partial v_y}{\partial y}\right),$$

where ρ is the density of the medium; λ and μ are the Lamé constants; v_x and v_y are the horizontal and vertical velocities of the medium particles; and σ_{xx}, σ_{yy}, and σ_{xy} are stress tensor components.

This system can be rewritten in matrix form:

$$\frac{\partial u_p}{\partial t} + A_{pq}\frac{\partial u_q}{\partial x} + B_{pq}\frac{\partial u_q}{\partial y} = 0, \tag{1}$$

where $\mathbf{u}$ is the vector of five independent variables: $\mathbf{u} = (\sigma_{xx}, \sigma_{yy}, \sigma_{xy}, v_x, v_y)^{\mathrm{T}}$. Closed-form expressions for the matrices A_{pq} and B_{pq} can be found in [27]. Here and below, summation over repeated indices is implied. The eigenvalues of A_{pq} and B_{pq} are $s_1 = -c_p$, $s_2 = -c_s$, $s_3 = 0$, $s_4 = c_s$, and $s_5 = c_p$, where c_p and c_s are the respective velocities of propagation of P- and S-waves in the medium. Below, we briefly describe the numerical methods to be compared.

1.1. Discontinuous Galerkin Method

Assume that the integration domain is partitioned into triangular cells $T^{(m)}$ and the matrices A_{pq} and B_{pq} are constant inside $T^{(m)}$. In each cell, the solution of system (1) is numerically approximated by a linear combination of $\frac{1}{2}(N+1)(N+2)$ time-independent polynomial functions $\Phi_k(x, y)$ of degrees at most N (which form a basis supported by $T^{(m)}$) with time-dependent coefficients:

$$\hat{u}_{pl}^{(m)}(t) : (u_h^{(m)})_p(x, y, z) = \hat{u}_{pl}^{(m)}(t)\Phi_l(x, y). \tag{2}$$

Multiplying (1) by the basis function Φ_k and integrating the result over the triangle $T^{(m)}$, we obtain

$$\int\limits_{T^{(m)}} \Phi_k \frac{\partial (u_h)_p}{\partial t} dV + \int\limits_{T^{(m)}} \Phi_k \left(A_{pq}\frac{\partial (u_h)_q}{\partial x} + B_{pq}\frac{\partial (u_h)_q}{\partial y}\right) dV = 0. \tag{3}$$

Next, applying the integration-by-parts formula yields

$$\int\limits_{T^{(m)}} \Phi_k \frac{\partial (u_h)_p}{\partial t} dV + \sum_{j=1}^{3} \int\limits_{(\partial T^{(m)})_j} \Phi_k F_p^{h,j} dS - \int\limits_{T^{(m)}} \left(\frac{\partial \Phi_k}{\partial x} A_{pq}(u_h)_q + \frac{\partial \Phi_k}{\partial y} B_{pq}(u_h)_q\right) dV = 0. \tag{4}$$

The second term appears since the solution u_h and the matrices A_{pq} and B_{pq} are generally discontinuous on the boundary of $T^{(m)}$. Here, $F_p^{h,j}$ is the numerical flux through the jth edge of $T^{(m)}$ in a global coordinate system and $(\partial T^{(m)})_j$ denotes the sides of $T^{(m)}$, $j = 1, 2, 3$.

Let $T_{pq}^{m_j}$ be the transition matrix to a coordinate system $X'Y'$ associated with the jth edge of $T^{(m)}$ (the transformation is orthogonal). Then the flux $F_p^{h,j}$ can be approximately found as

$$F_p^{h,j} = T_{pq}^{m_j} A_{ql} u_l^{\downarrow}, \tag{5}$$

where $u_l^{\downarrow}$ is the solution of the one-dimensional Riemann problem, which can be obtained analytically by applying the Rankine–Hugoniot jump condition to each characteristic and taking into account that the velocity and the force density are continuous at the contact in the case of the no-slip contact condition. Slip and dry friction conditions can also be set at the contact.

Expressions (2), (4), and (5) represent a semidiscrete numerical scheme. A more detailed derivation can be found in [28, 8, 29]. The time differencing is based on a high-order accurate Runge–Kutta method, which is fully local and well suited for parallelization. As a system of basis polynomials, we use the orthogonal Dubiner polynomials of fifth order, while the fifth-order Dormand–Prince method with an adaptive step is used as an integrator.

1.2. Grid-Characteristic Method on Unstructured Meshes

By applying coordinate splitting, the design of a difference scheme for system (l) can be reduced to the construction of a difference scheme for a system of the form

$$\frac{\partial u_p}{\partial t} + A_{pq}\frac{\partial u_q}{\partial x} = 0. \tag{6}$$

For hyperbolic system (6), the matrix $\mathbf{A}$ can be represented as $\mathbf{A} = \mathbf{R}\Lambda\mathbf{R}^{-1}$, where Λ is a diagonal matrix with elements being the eigenvalues of $\mathbf{A}$, while $\mathbf{R}$ is a matrix consisting of the right eigenvectors of $\mathbf{A}$. After introducing the new variables $\mathbf{w} = \mathbf{R}^{-1}\mathbf{u}$ (Riemann invariants), system (6) is reduced to a system of five independent scalar transport equations. To obtain the solution of the transport equation at the point (x_m, y_m) at the time t_n, we draw a corresponding characteristic through this point and find the intersection point $(\tilde{x}_m, \tilde{y}_m)$ of this characteristic with the previous time level ($t = t_{n-1}$). Since the solution remains unchanged along the characteristic, it remains to approximate the solution at the point $(\tilde{x}_m, \tilde{y}_m)$ at $t = t_{n-1}$.

There are several methods for interpolation in a triangle that are used in the theory of grid-characteristic methods. The simplest one is to choose the required number of additional points on the boundary of a triangle or inside it and to use them in interpolation based on an Nth-degree polynomial [30]. Note that monotonization may be required for interpolation of order higher than the first (for more details on monotonization methods, see [31]).

After finding the Riemann invariants at the next time step, the solution is recovered as

$$\mathbf{u}^{n+1} = \mathbf{R}\mathbf{w}^{n+1}. \tag{7}$$

In the theory of grid-characteristic methods, contacts are usually treated in a shock-fitting manner by specifying boundary conditions in explicit form [11, 18]. In this paper, we use a shock-capturing grid-characteristic method, which has a number of advantages over the shock-fitting technique; specifically, it is simpler and faster as applied to media with a large number of interfaces.

Let us describe the algorithm for computing transport equations on triangular meshes by applying the shock-capturing grid-characteristic method. In this case, neighboring cells may have different physical parameters, so we have to introduce special combined matrices of transition to Riemann invariants that take into account the characteristics of both contacting cells. Let the cell reached by characteristics with positive eigenvalues and all corresponding parameters (including the matrices $\mathbf{A}$ and $\mathbf{R}$) be denoted by R. The cell reached by characteristics with negative eigenvalues is denoted by L (Fig. 1).

A numerical step can be divided into the following three stages.

1. Find the Riemann invariants by using the combined matrix $\mathbf{R}^{-1}$: $\mathbf{w}_m^n = \mathbf{R}^{-1}\mathbf{u}_m^n$.

2. Approximate values for Riemann invariants at four points, $c_1\mathbf{n}_1$, $c_2\mathbf{n}_1$, $c_1\mathbf{n}_2$, and $c_2\mathbf{n}_2$, to obtain $\mathbf{w}_m^{n+1}$.

3. Find $\mathbf{u}_m^{n+1}$ with the help of the combined matrix $\mathbf{R}$: $\mathbf{u}_m^{n+1} = \mathbf{u}_m^n + \mathbf{R}(\mathbf{w}_m^{n+1} - \mathbf{w}_m^n)$.

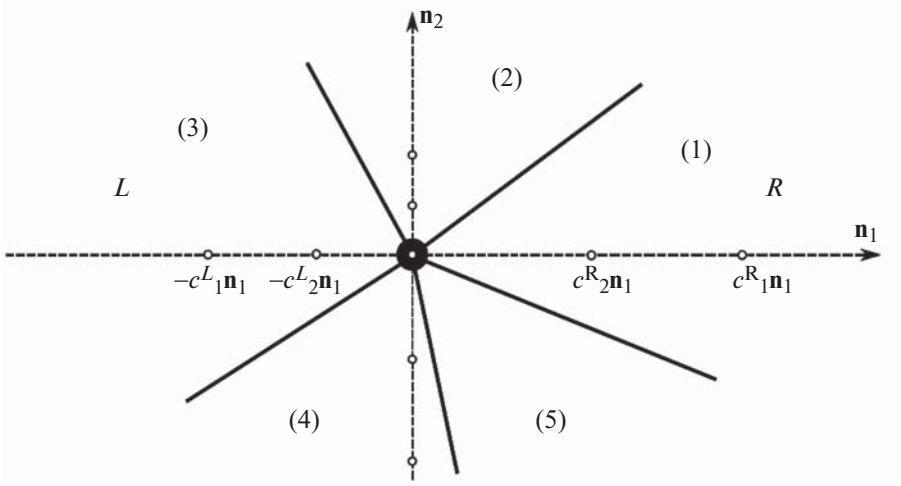

Fig. 1. Schematic of the shock-capturing grid-characteristic scheme on an unstructured (triangular) mesh. The physical parameters of neighboring triangles are generally different. The intersections of the characteristics with the preceding time level are marked.

According to [32], we use the combined matrix $\mathbf{R}^{-1}$ with rows determined by the cell at which the corresponding characteristic arrives:

$$\mathbf{R}^{-1} = \begin{pmatrix} \mathbf{l}^0_{\lambda=0} \\ \mathbf{l}^L_{\lambda=-c_2} \\ \mathbf{l}^R_{\lambda=c_2} \\ \mathbf{l}^L_{\lambda=-c_1} \\ \mathbf{l}^R_{\lambda=c_1} \end{pmatrix} = \begin{pmatrix} c_3^0/c_1^0 & 1 & 0 & 0 & 0 \\ 1/(2c_{1L}\rho_L) & 0 & 0 & 1/2 & 0 \\ -1/(2c_{1R}\rho_R) & 0 & 0 & 1/2 & 0 \\ 0 & 0 & 1/(2c_{2L}\rho_L) & 0 & 1/2 \\ 0 & 0 & 1/(2c_{2R}\rho_R) & 0 & 1/2 \end{pmatrix}, \tag{8}$$

where $\mathbf{l}^L_i$ and $\mathbf{l}^R_i$ are the left eigenvectors of the matrices $\mathbf{A}_L$ and $\mathbf{A}_R$, respectively, and $c_3 = (c_1^2 - 2c_2^2)/c_1$. Here, c_1^0 and c_3^0 are approximations of physical parameters at a given point rather than in a cell. In this work, they are approximated as $c_1^0 = (c_{1L} + c_{1R})/2$ and $c_2^0 = (c_{2L} + c_{2R})/2$. The transition matrix from the Riemann invariants to the original variables is found by inverting matrix (8).

Unfortunately, efficient stable grid-characteristic schemes of order higher than the second are available only on structured meshes.

1.3. Shock-Capturing Grid-Characteristic Method on Structured Meshes

The implementation of the grid-characteristic method on structured meshes is similar in many respects to that on unstructured meshes. By coordinate splitting, the solution of system (1) is reduced to the sequential solution of one-dimensional systems of form (6). Then the transition to Riemann invariants is performed as described above. As a result, the problem is reduced to one-dimensional transport equations. They were numerically integrated using the grid-characteristic schemes described in [31].

The code incorporates second- to fourth-order accurate schemes. Most of the computations were based on a third-order accurate scheme.

As applied to the one-dimensional linear transport equation $u_t + au_x = 0$ with $a > 0$, this scheme is given by

$$\begin{gathered} u_m^{n+1} = u_m^n + \sigma(\Delta_0 + \Delta_2)/2 + \sigma^2(\Delta_0 - \Delta_2)/2 + \frac{\sigma(\sigma^2 - 1)}{6}(\Delta_1 - 2\Delta_0 + \Delta_2), \\ \Delta_0 = u_{m-1}^n - u_m^n, \\ \Delta_1 = u_{m-2}^n - u_{m-1}^n, \\ \Delta_2 = u_m^n - u_{m+2}^n, \end{gathered} \tag{9}$$

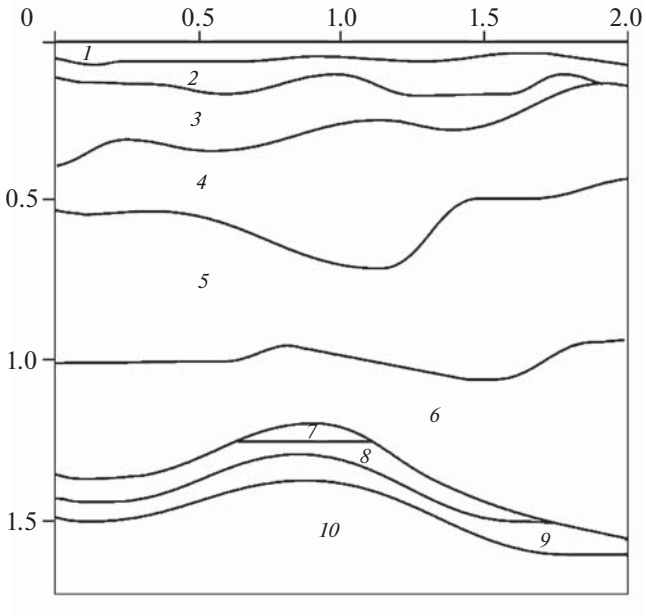

Fig. 2. Anticlinal trap model.

where $\sigma = a\tau/h$, τ is the time step, and h is the spatial mesh size. Scheme (9) is stable for Courant numbers not exceeding 1 and is third-order accurate in space and time. For monotonization, we use a grid-characteristic monotonicity criterion [31] relying on the characteristic property of the exact solution:

$$\min(u_{m-1}^n, u_m^n) \le u_m^{n+1} \le \max(u_{m-1}^n, u_m^n).$$

In places where this criterion holds, the order of the scheme is reduced to the second.

After the transport equation has been numerically integrated, the transition to physical variables of the original system is performed by multiplying the Riemann invariants by the inverse of matrix (8). The transition to Riemann invariants and the return to the original variables occur at every iteration step of the time-stepping procedure.

2. NUMERICAL EXPERIMENT

2.1. Formulation

As a geological model, we use an anticlinal trap [1] with numerous contact surfaces, which represents a typical hydrocarbon deposit (see Fig. 2). Due to the trap structure, the seismogram involves multiple waves, which have to be separated from the useful signal, a task that can hardly be performed with low-order numerical schemes. The sizes of the domain are indicated in kilometers. The parameters of the layers are given in Table 1.

A nonreflecting boundary condition was specified on the lower and lateral boundaries, while a free boundary was set at the top of the domain. The perturbation source was defined as a vertical force applied to an area from 925.7 to 974.1 m on the daytime surface with an amplitude described by a 40-Hz Ricker wavelet.

Seismic data were recorded at a depth of 40 cm from the daytime surface (with 99 sensors distributed uniformly from 20 to 1980 m). For a more detailed comparison, we used the 47th wave path (indexing starts at 1) at the point $x = 940$ m.

2.2. Comparison of Results

The grids were constructed so as to simulate waves in the range 10–80 Hz. The minimum wavelength (and, hence, the finest grid) was determined by the relation $\lambda_{\min} = V_{\min}/f_{\max} = 1.6 \times 10^3/80 = 20$ m. The computational domain was discretized so that the wavelength was covered by least 5–10 points [33, 34].

Table 1. Parameters of the layers in the geological model

Layer	Parameters		
	c_p (km/s)	c_s (km/s)	ρ (g/cm^3)
1	2.6	1.6	2.1
2	3.2	1.96	2.3
3	3.7	2.26	2.3
4	4	2.45	2.4
5	4.3	2.63	2.5
6	4.5	2.75	2.6
7	3.2	1.7	2.3
8	4.6	2.82	2.6
9	4.8	2.94	2.7
10	5.4	3.3	2.8

Table 2. Comparison of the methods in terms of runtime

Method	Runtime per degree of freedom, μs
DGM	6×10^{-1}
GCM Structured	1×10^{-2}
GCM Unstructured	6

Relying on these requirements, uniform grids were constructed for all three methods. For example, for DGM, in the case of fifth-order polynomials, it was sufficient to use $\approx 2 \times 10^4$ triangles (with five points per wavelength) without taking into account the constraints on the geometry of the layers in the problem. In view of the geometry, the number of triangles was increased to $\approx 4 \times 10^4$. For the second-order GCM Unstructured, we used $\approx 1.5 \times 10^6$ triangles. For the GCM Structured, the grid was uniform in both directions and consisted of 2000×1722 or $\approx 3.4 \times 10^6$ cells.

Table 2 gives the runtime for each the methods. All the characteristics were normalized by the number of degrees of freedom to make the comparison more objective, since the methods have different orders. Let us explain the method for computing the runtime required for a single degree of freedom in the case of DGM. One step of the fourth-order Runge–Kutta algorithm in the case of sixth-order polynomials and 98916 triangles requires time of 6.7 s on one core of an Intel (R) Xeon (R) CPU E5-2620 v2 @ 2.1 GHz processor. Then, by normalizing the single-step runtime by the number of integration stages, the number of degrees of freedom per cell $\frac{1}{2}(N+1)(N+2)$, the number of cells, and the number of kernels, we obtain 6×10^{-1} μs. For the third-order GCM Structured, the runtime was normalized by $3^2 = 9$, which corresponds to a grid for a first-order scheme with nine times more nodes.

The storage was not compared, since its normalized value is identical for all methods and is equal to the number of unknowns (five) times the floating-point number size. It should be emphasized that somewhat more degrees of freedom is necessary for DGM to achieve the same accuracy as in GCM, because the solution on a cell boundary is discontinuous and the number of degrees of freedom over the perimeter of the cell doubles, but the total effect of this is insignificant in comparison with the total amount of storage.

It is difficult to compare numerical methods that are so different in nature. The runtime per one degree of freedom (see Table 2) depends not only on the method used, but, to a higher degree, on its implementation. Judging from the number of operations required for one degree of freedom, GCM Structured is the fastest method, GCM Unstructured is the next, and DGM is theoretically the slowest of all. Additionally, each method has its own distinctive features. For example, for DGM with Nth-order polynomials, the order of convergence in space is $N + 1$. For GCM, the order of interpolation coincides with the order of convergence in space and time. The time step constraint for methods on unstructured meshes is usually

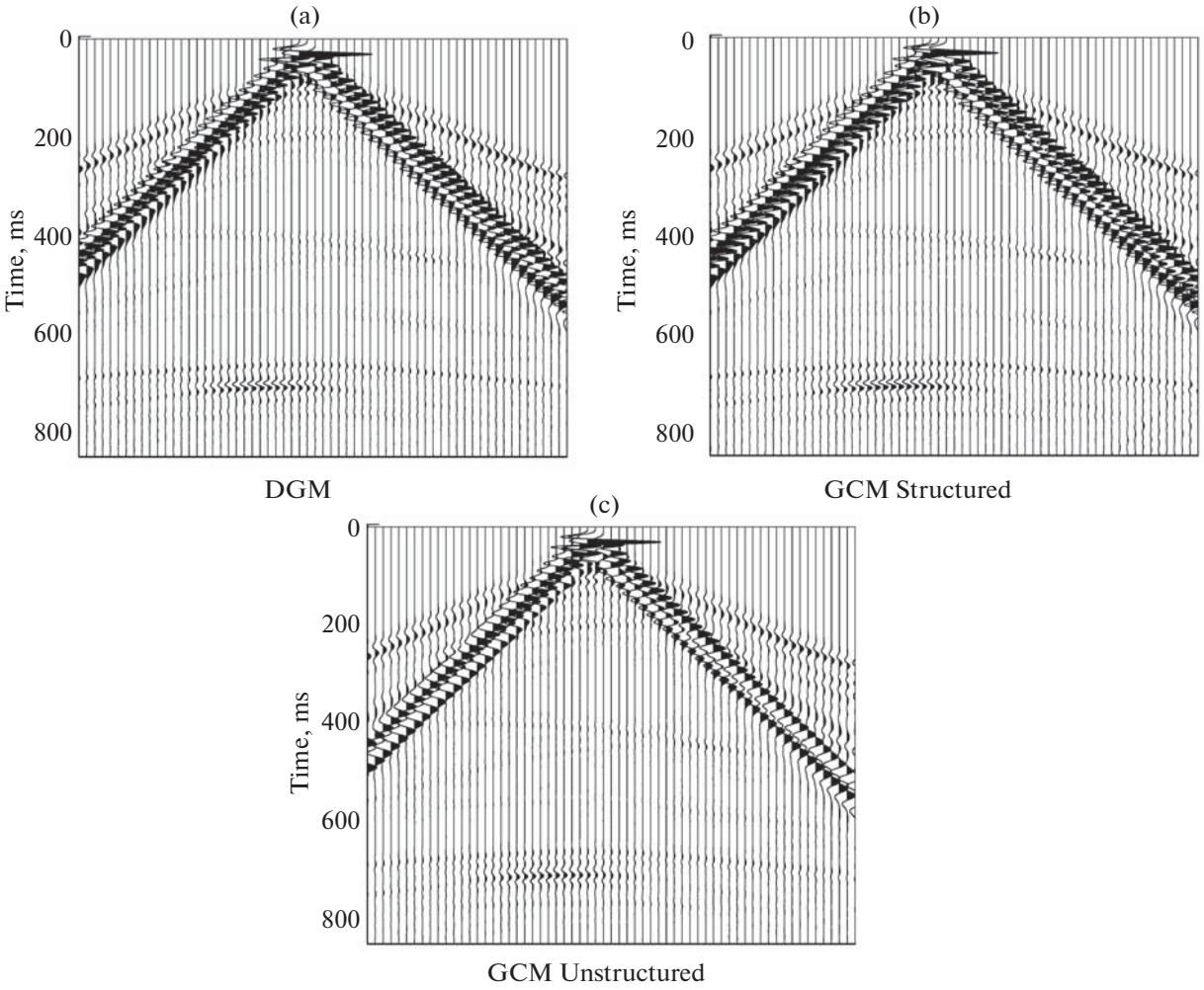

Fig. 3. Vertical velocity seismograms produced by the discontinuous Galerkin method and the grid-characteristic method on structured and unstructured meshes.

written as $\Delta t = \min_i \frac{1}{N} \frac{h_i}{c_p^i}$, where h_i is the minimum height of the ith cell. Therefore, such low-order methods require fewer integration steps, while the multiplier $1/N$ is missing in GCM Structured and many other methods on structured meshes. Additionally, in some cases, the steps in space and time in GCM Structured can be chosen so that the solution is "transferred" from the preceding time step without interpolation, i.e., the characteristics pass through the nodes.

Figure 3 shows the seismograms obtained with the help of three methods. Qualitatively, they are in complete agreement in terms of amplitudes and phases. A more detailed inspection of their central domains, which carry information on the location of the anticlinal trap (see Fig. 4), reveals small differences in the phases and amplitudes of the recorded signals: the maximum difference in time between the recorded signals is 1.2 ms for DGM and GCM Structured and 3.8 ms for DGM and GCM Unstructured. The maximum difference between the amplitudes of the vertical component is 4% for DGM and GCM Structured and 11% for DGM and GCM Unstructured. This difference for GCM Unstructured is explained by the fact that it has lower (second-order) accuracy than the other methods.

Figure 5 displays the wave pattern at $t = 0.38$ s. The velocity amplitude of medium particles is shown in shades of gray. The response to the anticlinal trap is clearly seen in the central domain.

Figure 6 compares the vertical velocity component for the 47th wave path (sensor is at the point (940 m, –0.4 m)). DGM and GCM Structured have identical signal shapes (phase relations), but the

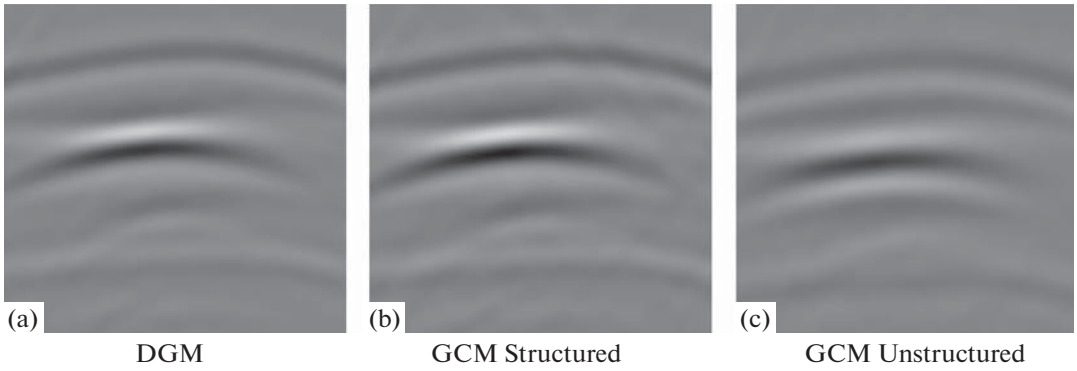

Fig. 4. Detailed response to the anticlinal trap in the vertical velocity seismograms derived by the discontinuous Galerkin method and the grid-characteristic method on structured and unstructured meshes.

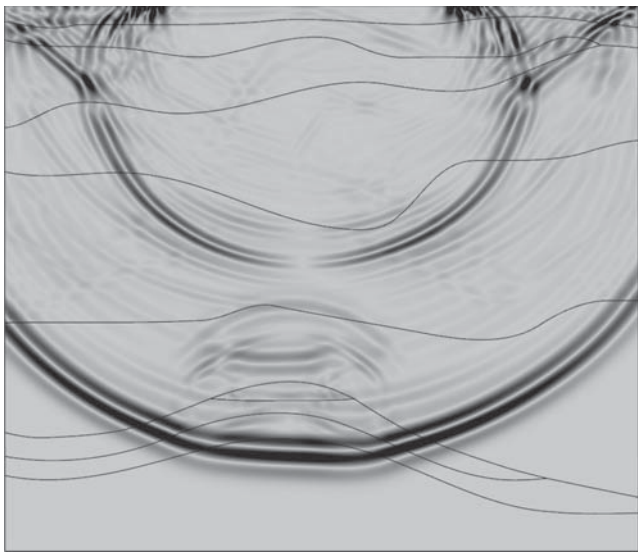

Fig. 5. Wave pattern at $t = 0.38$ s.

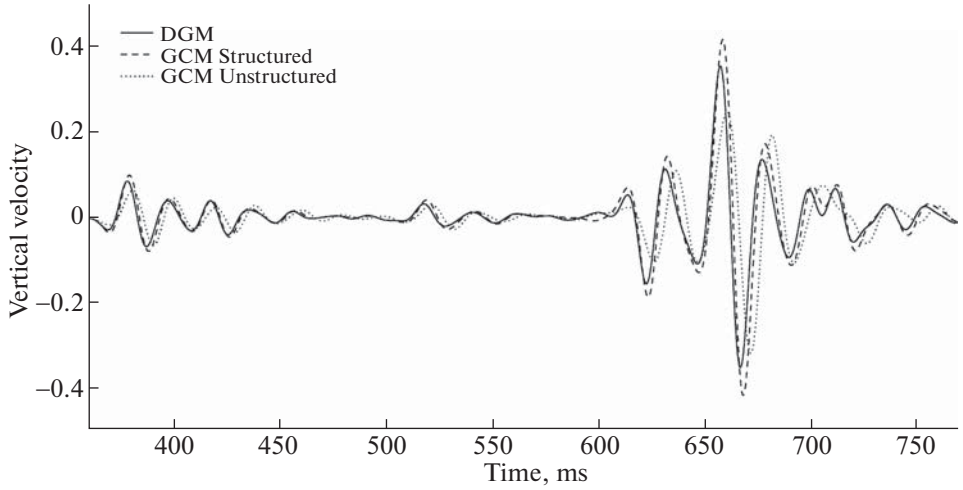

Fig. 6. Comparison of wave path data at the point (940 m, –0.4 m).

amplitudes of the signals differ by 15%. The maximum difference between DGM and GCM Unstructured amounts to 10%, which is explained by the difference in the accuracy of these methods.

CONCLUSIONS

Three high-order numerical methods were considered. Previously, it was shown in a number of studies that, at a fixed level of errors, high-order methods are more efficient in terms of required resources than low-order methods on finer grids [35]. The wave patterns computed for the anticlinal trap model by applying three methods showed that the amplitudes and phases of signals recorded on the daytime surface coincide to a high degree. All three numerical methods and their software implementations are suitable for field data computations. GCM Structured is much more efficient, since it requires fewer operations per one degree of freedom and has a more efficient implementation on modern computers due to the density of data.

It was shown that, despite its rectangular mesh discretization, GCM Structured yields results comparable with those produced by the unstructured mesh methods. This is achieved by using a larger number of nodes, which is compensated for by the higher computation speed. These results agree with the conclusions drawn in [36, 37]. Nevertheless, unstructured-mesh methods might be preferable in the simulation of complex-structured objects, when methods on structured meshes lead to large errors in the approximation of the geometry of the computational domain. A comparison of this kind is intended to be made in future works.

ACKNOWLEDGMENTS

This work was supported by the Russian Science Foundation, project no. 14-11-00263.

REFERENCES

1. J. M. Carcione, G. C. Herman, and A. P. E. Ten Kroode, "Seismic Modeling," Geophysics **67** (4), 1304–1325 (2002).
2. J. Virieux, H. Calandra, and R. É. Plessix, "A review of the spectral, pseudo-spectral, finite-difference and finite-element modeling techniques for geophysical imaging," Geophys. Prospect. **59** (5), 794–813 (2011).
3. J. Virieux, V. Etienne, et al., "Modeling seismic wave propagation for geophysical imaging," *Seismic Waves: Research and Analysis* (InTech, 2012), pp. 253–304.
4. P. Moczo, J. Kristek, and M. Galis, *The Finite-Difference Modeling of Earthquake Motions: Waves and Ruptures* (Cambridge Univ. Press, Cambridge, 2014).
5. W. Nowacki, *Teoria sprężystości* (Panstwowe Wydawn. Naukowe, 1970; Mir, Moscow, 1975).
6. V. Etienne, E. Chaljub, et al., "An hp-adaptive discontinuous Galerkin finite-element method for 3D elastic wave modeling," Geophys. J. Int. **183** (2), 941–962 (2010).
7. V. Hermann, M. Käser, and C. E. Castro, "Non-conforming hybrid meshes for efficient 2-D wave propagation using the discontinuous Galerkin method," Geophys. J. Int. **184** (2), 746–758 (2011).
8. V. A. Miryakha, A. V. Sannikov, and I. B. Petrov, "Discontinuous Galerkin method for numerical simulation of dynamic processes in solids," Math. Model. Comput. Simul. **7** (5), 446–455 (2015).
9. E. D. Mercerat and N. Glinsky, "A nodal high-order discontinuous Galerkin method for elastic wave propagation in arbitrary heterogeneous media," Geophys. J. Int. **201** (2), 1099–1116 (2015).
10. F. B. Chelnokov, "Explicit representation of grid-characteristic schemes for elasticity equations in 2D and 3D spaces," Mat. Model. **18** (6), 96–108 (2006).
11. I. E. Kvasov, S. A. Pankratov, and I. B. Petrov, "Numerical simulation of seismic responses in multilayer geologic media by the grid-characteristic method," Math. Model. Comput. Simul. **3** (2), 196–204 (2011).
12. I. B. Petrov, A. V. Favorskaya, et al., "Grid-characteristic method using high-order interpolation on tetrahedral hierarchical meshes with a multiple time step," Math. Model. Comput. Simul. **5** (5), 409–415 (2013).
13. V. I. Golubev, I. B. Petrov, and N. I. Khokhlov, "Simulation of seismic processes inside the planet using the hybrid grid-characteristic method," Math. Model. Comput. Simul. **7** (5), 439–445 (2015).
14. V. I. Golubev, I. B. Petrov, et al., "Numerical computation of wave propagation in fractured media by applying the grid-characteristic method on hexahedral meshes," Comput. Math. Math. Phys. **55** (3), 509–518 (2015).
15. I. B. Petrov, A. V. Favorskaya, et al., "Monitoring the state of the moving train by use of high performance systems and modern computation methods," Math. Model. Comput. Simul. **7** (1), 51–61 (2015).
16. I. E. Kvasov and I. B. Petrov, "High-performance computer simulation of wave processes in geological media in seismic exploration," Comput. Math. Math. Phys. **52** (2), 302–313 (2012).

17. I. E. Kvasov, V. B. Levyant, and I. B. Petrov, "Numerical simulation of direct responses to sheet zones with subvertical fluid-saturated mesofractures," Tekhnol. Seismorazvedki, No. **3**, 19–35 (2013).
18. V. I. Golubev, I. B. Petrov, and N. I. Khokhlov, "Numerical simulation of seismic activity by the grid-characteristic method," Comput. Math. Math. Phys. **53** (10), 1523–1533 (2013).
19. I. B. Petrov and N. I. Khokhlov, "Modeling 3D seismic problems using high-performance computing systems," Math. Model. Comput. Simul. **6** (4), 342–350 (2014).
20. R. Versteeg, "The Marmousi experience: Velocity model determination on a synthetic complex data set," The Leading Edge **13**, 927–936 (1994).
21. G. S. Martin, R. Wiley, and K. J. Marfurt, "Marmousi2: An elastic upgrade for Marmousi," The Leading Edge **25** (2), 156–166 (2006).
22. J. D. De Basabe and K. Sen Mrinal, "New developments in the finite-element method for seismic modeling," The Leading Edge **28** (5), 562–567 (2009).
23. C. E. Castro, M. Käser, and G. B. Brietzke, "Seismic waves in heterogeneous material: Subcell resolution of the discontinuous Galerkin method," Geophys. J. Int. **182** (1), 250–264 (2010).
24. S. Wenk, C. Pelties, et al., "Regional wave propagation using the discontinuous Galerkin method," Solid Earth **4** (1), 43–57 (2013).
25. J. Robertsson, R. Laws, et al., "Modeling of scattering of seismic waves from a corrugated rough sea surface: A comparison of three methods," Geophys. J. Int. **167** (1), 70–76 (2006).
26. P. Moczo, J. Kristek, et al., "3-D finite-difference, finite-element, discontinuous-Galerkin and spectral-element schemes analyzed for their accuracy with respect to P-wave to S-wave speed ratio," Geophys. J. Int. **187** (3), 1645–1667 (2011).
27. R. J. LeVeque, *Finite Volume Methods for Hyperbolic Problems* (Cambridge University Press, New York, 2002).
28. M. Käser and M. Dumbser, "An arbitrary high-order discontinuous Galerkin method for elastic waves on unstructured meshes. I: The two-dimensional isotropic case with external source terms," Geophys. J. Int. **166** (2), 855–877 (2006).
29. L. Wilcox and G. Stadler, et al., "A high-order discontinuous Galerkin method for wave propagation through coupled elastic-acoustic media," J. Comput. Phys. **229** (24), 9373–9396 (2010).
30. P. I. Agapov and F. B. Chelnokov, "Comparative analysis of difference schemes for the numerical solution of 2D problems in solid mechanics," in *Simulation and Data Processing: Collected Papers* (Mosk. Fiz. Tekh. Inst., Moscow, 2003), pp. 19–27.
31. A. S. Kholodov and Ya. A. Kholodov, "Monotonicity criteria for difference schemes designed for hyperbolic equations," Comput. Math. Math. Phys. **46** (9), 1560–1588 (2006).
32. A. G. Kulikovskii, N. V. Pogorelov, and A. Yu. Semenov, *Mathematical Aspects of Numerical Solution of Hyperbolic Systems* (Fizmatlit, Moscow, 2001; Chapman and Hall/CRC, London, 2001).
33. D. Komatitsch, "The spectral-element method in seismology," Geophys. Monograph Ser. **157**, 205–227 (2005).
34. J. D. De Basabe and M. K. Sen, "Grid dispersion and stability criteria of some common finite-element methods for acoustic and elastic wave equations," Geophysics **72** (6), T81–T95 (2007).
35. M. Käser and M. Dumbser, "A highly accurate discontinuous Galerkin method for complex interfaces between solids and moving fluids," Geophysics **73** (3), T23–T35 (2008).
36. C. Pelties, M. Käser, et al., "Regular versus irregular meshing for complicated models and their effect on synthetic seismograms," Geophys. J. Int. **183** (2), 1031–1051 (2010).
37. G. Bono and A. M. Awruch, "Numerical study between structured and unstructured meshes for Euler and Navier–Stokes equations," Mec. Comput. **26**, 3134–3146 (2007).

Translated by I. Ruzanova

SPELL: OK